Article

Acid Resistance of Alkali-Activated Natural Pozzolan and Limestone Powder Mortar

Khaled A. Alawi Al-Sodani [1,*], Adeshina A. Adewumi [1,*], Mohd Azreen Mohd Ariffin [2],
Babatunde Abiodun Salami [3], Moruf O. Yusuf [1], Mohammed Ibrahim [4], Ali H. AlAteah [1],
Mohammed M. H. Al-Tholaia [1], Sami M. Ibn Shamsah [5] and Mohammad Ismail [2]

1   Department of Civil Engineering, College of Engineering, University of Hafr Al Batin, P.O. Box 1803,
    Hafr Al Batin 39524, Saudi Arabia
2   Faculty of Engineering, School of Civil Engineering, Universiti Teknologi Malaysia,
    Johor Bahru 81310, Malaysia
3   Interdisciplinary Research Center for Construction and Building Materials, Research Institute,
    King Fahd University of Petroleum and Minerals, Dhahran 31261, Saudi Arabia
4   Applied Research Center for Metrology, Standards and Testing, Research Institute,
    King Fahd University of Petroleum and Minerals, Dhahran 31261, Saudi Arabia
5   Department of Mechanical Engineering, College of Engineering, University of Hafr Al Batin, P.O. Box 1803,
    Hafr Al Batin 39524, Saudi Arabia
*   Correspondence: kalsodani@uhb.edu.sa (K.A.A.A.-S.); adeshina@uhb.edu.sa (A.A.A.);
    Tel.: +966-1372-05171 (K.A.A.A.-S.)

Abstract: The development of sustainable, environmentally friendly alkali-activated binder has emerged as an alternative to ordinary Portland cement. The engineering and durability properties of alkali-activated binder using various precursor combinations have been investigated; however, no study has focused on the impact of high-volume natural pozzolan (NP) on the acid resistance of alkali-activated NP and limestone powder. Therefore, the current study assesses the impact of high-volume natural pozzolan (volcanic ash) on the durability properties of alkali-activated natural pozzolan (NP) and limestone powder (LSP) mortar by immersion in 6% H_2SO_4 for 365 days. The samples were prepared with different binder ratios using alkaline activators (10 M $NaOH_{(aq)}$ and Na_2SO_4) combined in a 1:1 ratio and cured at 75 °C. NP was combined with the LSP at three different combinations: NP:LSP = 40:60 ($AAN_{40}L_{60}$), 50:50 ($AAN_{50}L_{50}$), and 60:40 ($AAN_{60}L_{40}$), representing low-volume, balanced, and high-volume binder combinations. Water absorption, weight change, and compressive strength were examined. The microstructural changes were also investigated using FTIR, XRD, and SEM/EDS characterization tools. Visual examination showed insignificant deterioration in the sample with excess natural pozzolan ($AAN_{60}L_{40}$) after 1 year of acid exposure, and the maximum residual strengths were 20.8 MPa and 6.68 MPa in $AAN_{60}L_{40}$ and $AAN_{40}L_{60}$ with mass gain (1.37%) and loss (10.64%), respectively. The high sulfuric acid resistance of $AAN_{60}L_{40}$ mortar was attributed to the high Ca/Si = 10 within the C-A-S-H and N-A-S-H formed. The low residual strength recorded in $AAN_{40}L_{60}$ was a result of gypsum formation from an acid attack of calcium-dominated limestone powder. The controlling factor for the resistance of the binder to acid corrosion was the NP/LSP ratio, whose factor below 0.6 caused significant debilitating effects.

Keywords: natural pozzolan; limestone powder; acid resistance; sulfuric acid; alkali activation

1. Introduction

Civil infrastructure deterioration due to industrial and biogenic acid attacks has been a cause of concern owing to the high cost of rehabilitation and retrofitting [1]. The resistance to acid of concrete structures is critical for long-term durability assessment and economic viability. In this context, cementitious materials with high acid resistance are required for various acid-exposed critical infrastructures to enhance their durability. Although the

ordinary Portland cement (OPC) binder is known to be resistant to chemical attacks, it is highly susceptible to acid attack through either the decomposition and leaching of hydration products or the negative effect of newly formed compounds on the binder's internal microstructure [2]. To improve the durability performance of OPC binders, researchers are constantly striving to produce better-performing binders through the modification of OPC binders via novel chemical or mineral admixtures, among other approaches. Mineral admixtures such as fly ash, silica-fume, ground granulated blast furnace slag, rice husk ash, silicomanganese, etc., are commonly used to increase the long-term durability of concrete through the formation of a uniform and consolidated internal matrix [3–11].

The development of alkali-activated materials (AAMs), which have been studied and shown to have better acid resistance than OPC, is another strategy adopted by researchers to develop durable materials [12,13]. The choice of source material, which has been shown to affect an AAM's internal structure, has a substantial impact on the durability performance of the AAM [14]. Relatively new [15–17] and old [12,13] studies have also confirmed that AAM offers superior durability performance in comparison to OPC binders. Although it is reported that AAMs outperform OPC binder in terms of durability, the quality of binder products required to resist acid attack depends on the calcium level in its source material [13]. The difference in the quality of the produced binder is responsible for significant variance in the durability test outcomes. The mechanism of deterioration, for instance, with varying exposure concentrations of acid, is significantly different [12,13,15]. As a result, there has been considerable skepticism about alkali-activated materials' superior durability performance in surviving the harshness of acids during exposure. However, new [16–18] and old [12,13] studies have confirmed AAMs' superior durability performance compared to OPC materials.

In a recent study, Reu et al. [16] investigated the degradation of slag/fly ash mortar (mixed in varying proportions) in an acidic medium comprising phosphoric and sulfuric acids at pH of 2.5 ± 0.5 for 150 days of exposure. The findings indicated variation in the aggressiveness of acid attack, with phosphoric acid being the most aggressive, and that the degradation level of AAM was far less than that of OPC-based mortar. Chen et al. [15] studied the durability performance of pavement repair mortar materials developed from alkali-activated metakaolin–GGBFS (MK-GGBFS) and OPC upon exposure to a strong sulfuric acid solution (pH = 1). The superior durability of the binary blend of alkali-activated MK-GGBFS over OPC was due to the void-filling effect and the formation of alkali-activated binder gel (N-A-S-H and C-S-H). The degradation of the mortar in the sulfuric acid environment was attributed to the leaching of metal cations, the breakdown of aluminosilicate bonds, and the formation of microcracks forming gypsum within the matrix [19]. In another comparative study [20], the resistance to acid solution of alkali-activated glass cullet (AAGC) synthesized from three types of recycled glasses (flat, hollow, and windshield) was reportedly better than that of OPC.

Many new materials have crept into the durability research space of alkali-activated materials; some of these materials include waste ceramic tile powder (WCP) [21,22], light-burnt dolomite powder [23], waste glass powder [24–26], volcanic ash [26], iron-rich laterite soil [27], silico-manganese fumes [28], glass cullet [20], palm oil fuel ash (POFA) [18], etc. Despite the different precursors, varied acid concentrations, and exposure durations, AAM's better performances were consistent in the reviewed comparative durability studies. This has encouraged researchers to explore other types of aluminosilicate precursors. Furthermore, 75 wt % of the Earth's crust is made up of silica and alumina, allowing for a significant number of raw materials, which could either be natural materials or waste by-products, available to be explored for alkaline activation [28].

Natural pozzolan (NP) is a siliceous or siliceous and aluminous material with a polymeric silicon–oxygen–aluminum framework. The alkali activation of NP involves the use of alkali activators ($NaOH_{(aq)}$ and $Na_2SiO_{3(aq)}$) for the hydrolysis and dissolution of complex aluminosilicate compounds present in NP. The dissolution process leads to the release of monomers such as Ca-O, Si-O-Si, Al-O-Al, and Al-O-Si. This pro-

cess is followed by the orientation of the oligomers, followed by the polycondensation of chains to form coagulated structures. Alkali activation of NP results in the formation of phillipsite ((Na,K,Ca)$_{1-2}$(Si,Al)$_8$O$_{16}$.6(H$_2$O)), CSH, calcium aluminum silicate hydrate ((Ca$_2$Al$_4$Si$_8$O$_{24}$)12H$_2$O), C-A-S-H), and sodium aluminosilicate hydroxide hydrate (Na$_8$(AlSiO$_4$)$_6$(OH)$_2$-4H$_2$O), N-A-S-H); these binder gels have been reported to enhance the strength development of the AAM [29,30].

Natural pozzolan (NP) is abundantly available in volcanic regions and is rich in silica content [31]. However, NP is deficient in CaO, which could cause a delay in the setting time of the binder. This has necessitated the binary blending of volcanic ash natural pozzolan and other CaO-containing waste, such as slag and limestone waste powder (LSP) [29,32]. LSP is generated during the tile production process; about 30 million tons are generated per year in Turkey, while the U.K. generates 22.2 million tons of LSP annually [29]. The synergy between NP and LSP as binary precursors in the development of the alkali-activated binder has enhanced the mechanical properties by improving microstructures [33].

There has been successful deployment of natural pozzolan (pumice, perlite, and volcanic ash) as a base material in alkali-activated binder, where its effect (either solely or supplemented with other materials) on mechanical and durability performance improvement has been reported [34–41]. However, these studies, especially on the durability performance of alkali-activated concrete AAC, either with NP alone or in combination with supplementary materials, are still limited. There are several studies on AAC durability against sulfate, acid attacks, diffusion, permeability, depth of oxygen and chloride ion penetration in NP-based binders [42–45]. In one of the studies on chloride ion transport in NP-based AAC, a high amount of chloride ions was recorded in the solution after the rapid chloride permeability test irrespective of the voltage applied [37,44]. However, improved or enhanced durability performance was recorded in the durability studies where NP was blended with other materials. For instance, in a recent work by Aguirre-Guerrero et al. [43], the corrosion behavior of blended NP/GBFS-based reinforced AAC exposed to a chloride-bearing environment was studied. Higher resistance to chloride ion penetration was recorded compared to ordinary Portland cement-reinforced concrete used as a control. This better performance was attributed to improved gel composition, microstructural characteristics, and the matrix's capacity to bind the chloride ions before reaching the rebar surface.

In another NP blended study, Ibrahim et al. assessed the acid resistance of NP blended with nano-silica AAC subjected to 5% sulfuric acid. A reduction in specimen strength and weight was recorded with the blended NP in comparison with NP-based AAC and OPC-based concrete. The role played by the nano-silica, according to the authors, in achieving better microstructure leading to enhanced performance was due to hydration products such as C-A-S-H with increased absorption of aluminum ions into the binder matrix. The exposure to sulfuric acid resulted in the disintegration of the paste between the aggregates. Aside from sulfuric acid exposure, the curing temperature was also identified as a dominant factor in the performance of NP-based AAC. NP-based AAC cured at lower temperatures performed better during exposure to 5% sulfuric acid [39].

There have been studies conducted mostly on the fresh properties and strength development of AAC using NP and other emerging materials; an example is NP and limestone powder [33,45]. However, little is understood about its performance in terms of exposure to acid attacks. Thus, this research investigated the impact of high-volume volcanic ash natural pozzolan on the acid resistance of alkali-activated natural pozzolan and limestone powder. To explore the possibility of synthesizing a sustainable and durable blend of alkali-activated mortar using volcanic natural pozzolan and limestone powder, the hardened mortar was exposed to 6% sulfuric acid resistance for 3, 6, 9, and 12 months. The binder's morphology was examined through scanning electron microscopy–energy-dispersive spectroscopy (SEM/EDS), the difference in mineral phases was observed through X-ray diffraction (XRD), and changes in the frequency of vibration of different functional groups and their bond

characteristics were studied using Fourier transform infrared (FTIR) spectroscopy. The findings of this study can reduce the waste that leads to environmental and health hazards.

2. Materials and Methods

2.1. Materials

2.1.1. Natural Pozzolan and Limestone Powder

The natural pozzolan (NP) used for this research was volcanic ash from the coast of the Red Sea, Saudi Arabia, and was commercially acquired from a local company. The limestone rock was mined in large sizes from a limestone quarry site in Riyadh (Saudi Arabia) and was transported to a tile-making factory in Hafr Al-Batin, Saudi Arabia. The dust generated during the cutting process of producing tiles was used for this research work. The two base materials were initially oven-dried at $105 \pm 5\,°C$ for 24 h, after which they were sieved through a No. 200 sieve. A particle size analyzer (HELOS (H3533) and QUIXEL brand) was used to determine the particle size distributions of the precursor materials. The analyzer worked using laser scattering principles. The precursors were dispersed in distilled water using the wetting method; then, the system was vigorously agitated to avoid sedimentation. The characteristics of the raw materials (NP and LSP) are given in Table 1. The specific surface areas (BET) of precursors were determined with Micromeritics ASAP2020 using nitrogen gas adsorption. The surface of the powdered sample was cleared of all adsorbed gasses (outgassing process). Then, the sample was cryogenically cooled using liquid nitrogen, followed by dosing of nitrogen gas into the system at reduced pressure. X-ray fluorescence (XRF) spectrometry was used to determine the elemental compositions of precursors. An XRF machine works by sending radiation waves to the samples in an intense X-ray beam from a radioisotope source. The primary source of rays excites the sample by detaching the tightly bound inner shell electrons from the excited atoms of the samples. When the excited atoms are relaxed to the original state, a fluorescent X-ray is emitted. The energies of these emitted rays are detected using an energy-dispersive detector that identifies the elemental traces in the sample, while the intensity of the X-rays is used to determine the quantity of the elements. X-ray diffraction (XRD) is a rapid and simple technique for non-destructive characterizations of crystalline materials. The results were analyzed by MATCH XRD software using the COD database. The chemical compositions of NP and LSP from X-ray fluorescence (XRF) spectrometry are shown in Table 2. The test provides information especially on structures, phases, preferred crystal orientations, and structural parameters. The mineralogical composition and phase nature of PMs were explored using an XRD Bruker instrument, model d2-Phaser, with Cu Ka radiation (40 kV, 40 mA) by continuous scanning within an angle 2-theta range of 4–80° and at a scan speed of 2.5°/min.

Table 1. Physical characteristics of NP and LSP.

Materials	Specific Gravity	Volume Mean Diameter (μm)	Specific Surface Area (cm^2/g)	d_{90} (μm)	d_{50} (μm)	d_{10} (μm)
LSP	2.7	12.1	0.6	31.0	6.4	1.20
NP	2.3	5.8	3.1	11.6	4.8	1.4

Table 2. Chemical constituents of NP and LSP.

Oxide Components (%)	CaO	SiO$_2$	Al$_2$O$_3$	Fe$_2$O$_3$	MgO	Na$_2$O	K$_2$O	L.O.I
NP	2.0	74.0	13.0	1.5	0.5	4.0	5.0	5.0
LSP	94.1	2.5	0.8	1.2	0.6	-	0.3	44.0

2.1.2. Alkaline Activators

The alkali activator used for this study is a combination of 10 M $NaOH_{(aq)}$ (NS) and $NaSiO_{3(aq)}$ (SS), the SS contains H_2O: 62.11%, SiO_2: 29.13% and Na_2O: 8.76% with silica modulus, and SiO_2/Na_2O of 3.3. It should be noted that sodium hydroxide was made a day in advance of mixing in order to allow the solution to cool.

2.1.3. Aggregates

The fine aggregate used for this study was desert sand from dunes that met ASTM C33's gradation size requirements, as shown in Table 3. The fine aggregates' specific gravity in saturated surface dry conditions was 2.63, and its fineness modulus was 2.6.

Table 3. Physical characteristics of NP and LSP.

S/N	Sieve Size (mm)	Cumulative Passing (%)
1	9.6	100
2	4.75	95
3	2.63	81
4	1.18	50.5
5	0.6	25.4
6	0.3	6.2
7	0.15	1.9

2.1.4. Acid Solution

The acidic solution used for the durability test was concentrated 6% $H_2SO_{4(aq)}$ solution supplied by Ajax Finechem Pty Ltd. with a molar mass of 98.08 g and specific gravity of 1.84. The purity level was 96.5%.

2.2. Experimental Program

2.2.1. Mix Design for the Mortar Preparation

The mortar was produced with three different precursor combinations (NP:LSP = 40:60, 50:50, and 60:40). The mortar was developed using a mass ratio of $Na_2SiO_{3(aq)}/10$ M $NaOH_{(aq)}$ (SS/NH) = 1.0. The mixes were designated as AAN_xL_{100-x}, where x represents the percentage of NP present in the mix. The mix was designed to study the effect of a high volume of LSP ($AAN_{40}L_{60}$), an equal volume of NP and LSP ($AAN_{50}L_{50}$), and a high volume of NP ($AAN_{60}L_{40}$). A fine aggregate to binder ratio of 2.0 was maintained for all mixes. The ($NaOH_{(aq)} + Na_2SiO_{3(aq)}$)/(NP + LSP) ratio was maintained at 0.5, while free water was 10%. Table 4 depicts the mix proportions used for this research.

Table 4. Mix proportions in kg/m^3 of the developed mortar.

Mix No.	Mix ID	NP	LSP	NH Molarity	SS/NH	SS	SH	H$_2$O	Fine Aggregate
M1	$AAN_{60}L_{40}$	363.0	242.0	10	1.0	151.5	151.5	60.5	1210
M2	$AAN_{50}L_{50}$	302.5	302.5	10	1.0	151.5	151.5	60.5	1210
M3	$AAN_{40}L_{60}$	242.0	363.0	10	1.0	151.5	151.5	60.5	1210

2.2.2. Mortar Preparation

The required dry quantities of materials, shown in Table 4, were mixed with the Liya 5.0 L planetary bench mixer. The precursor was mixed with the fine aggregate for 3 min. The alkaline activators (10 $NaOH_{(aq)} + Na_2SiO_{3(aq)}$) and water were mixed to achieve a homogeneous mixture. The mix was then placed in a cube mold of $50 \times 50 \times 50$ mm^3, conforming to ASTM C109, followed by consolidation using a Liya vibrating table. The surface was then meticulously smoothed with a trowel, covered with a polythene sheet to stop moisture evaporation, and finally oven-dried for 24 h at 75 °C. The demolded samples were subsequently cured over the course of 28 days by curing at a laboratory temperature

of 20 ± 5 °C for strength development. The samples were then immersed in 6% $H_2SO_{4(aq)}$ for 12 months and tested for 3-, 6-, 9-, and 12-month residual strength and change in mass. The sample morphology, bond characterization, and mineral phases after immersion were examined using SEM/EDX, FTIR, and XRD analysis, respectively.

2.2.3. Evaluation of the Resistance to Acid

To evaluate the resistance of the developed alkaline-activated mortar to acid attack, a cubic sample of $50 \times 50 \times 50$ mm^3 was used. The impact of acid on the mortar under study was investigated using 6% H_2SO_4, which was prepared using distilled water. Before being submerged in the solution, the 28-day-old specimens were weighed. The samples were immersed for 365 days and the solution was changed every month to maintain a pH of 1 throughout the test. The performance of geopolymer mortar specimens was evaluated using physical observation and by measuring the loss in weight and the residual strength.

2.3. Evaluation Methods
2.3.1. Water Absorption

Absorption is a measure of pore spaces present in the matrix of a specimen. The determination of water absorption is usually performed by controlling the drying of specimens in an oven until a constant mass is achieved, which signifies the complete removal of existing moisture. Water absorption of binder specimens was determined following ASTM C-642, with the exception that the samples were dried in an oven at 75 °C (similar to curing temperature) for 24 h and their masses were recorded. The samples were then placed in water for 24 h and the masses of the samples were measured in surface-dried conditions. The water absorption was evaluated using Equation (1).

$$\text{Water absorption } (\%) = \frac{m_2 - m_1}{m_1} \times 100 \tag{1}$$

where m_1 is the average mass of the oven-dried specimen in air and m_2 is the average mass of the surface-dried specimen after immersion.

2.3.2. Weight Loss

To study the resistance to acid attack, the cubic sample of $50 \times 50 \times 50$ mm^3 of known original weight was fully immersed in 6% $H_2SO_{4(aq)}$ after 28 days of air-curing for 12 months. The solutions were changed every 30 days to keep the acidic solution's concentration at a pH level of 1. The loss in weight after 3, 6, 9, and 12 months of immersion was measured by sensitive weighing balance upon drying the sample surface water using a dry towel to ensure dry surface conditions. Three replicates were used for each measurement, and the average was determined. The results are recorded as shown in Equation (2).

$$\text{Percentage weight change } (\%) = \frac{W_2 - W_1}{W_2} \times 100 \tag{2}$$

where W_1 is the average surface-dried mass after immersion and W_2 is the average air-dried specimen before immersion.

2.3.3. Compressive Strength

The mortar compressive strength was determined according to ASTM C150 using a Liya compression testing machine with a uniform loading rate of 0.9 kN/s. The testing on three replicates was determined after 28 days of curing and 3, 6, 9, and 12 months after immersion in acidic solution. The loss in the compressive strength was determined using Equation (3).

$$\text{Loss in compressive strength (MPa)} = \frac{\sigma_2 - \sigma_1}{\sigma_2} \times 100 \tag{3}$$

where σ_1 is the average loss in compressive strength of the specimen before immersion and σ_2 is the average loss in compressive strength of the specimen after immersion.

2.3.4. Binder Products Characterization

The morphology of the binders before and after immersion in the acidic solution was examined with the JSM-5800LV SEM device using an accelerating voltage of 20 kV, while the elemental composition of each spectrum was determined with an energy-dispersive X-ray spectroscopic analyzer. The bonds and functional groups of the binder products were characterized using Perking Elmer 880 (KBr pellet technique) Fourier transform infrared (FTIR) spectroscopy.

3. Results and Discussion

3.1. Characterization of Precursors (NP and LSP)

Figure 1 shows the particle size distribution (PSD) curves for NP and LSP. LSP (Figure 1, LSP) had a mean particle size of 12.1 μm, whereas NP powder had a mean particle size of 5.8 μm (Figure 1, NP). Critical observation of the SEM shown in Figure 2 reveals that the geometry of the particles of the materials differs significantly. LSP is spherical in shape while NP is flaky. This points to the fact that the preponderance of NP over LSP will enhance the permeability due to the presence of more interstitial pores within the matrix of the binder, as shown in Figure 2. The excessive absorption in NP-dominated binder is equally evident in Figure 2. The NP contains a diffuse hump at $2\theta \approx 23°$, which indicates the amorphous nature of NP. NP consists of plagioclase (Ca, Na) $Al_2Si_2O_8$, microcline ($KAl_2Si_2O_8$), and quartz (SiO_3), as revealed in Figure 3. LSP is crystalline in nature and mostly contains quartz (SiO_2) with calcite ($CaCO_3$). The activation of NP and LSP resulted in the formation of N-A-S-H and C-A-S-H products, while the unreactive silica acts as a filler, thereby reducing the porosity of the resulting binder [29].
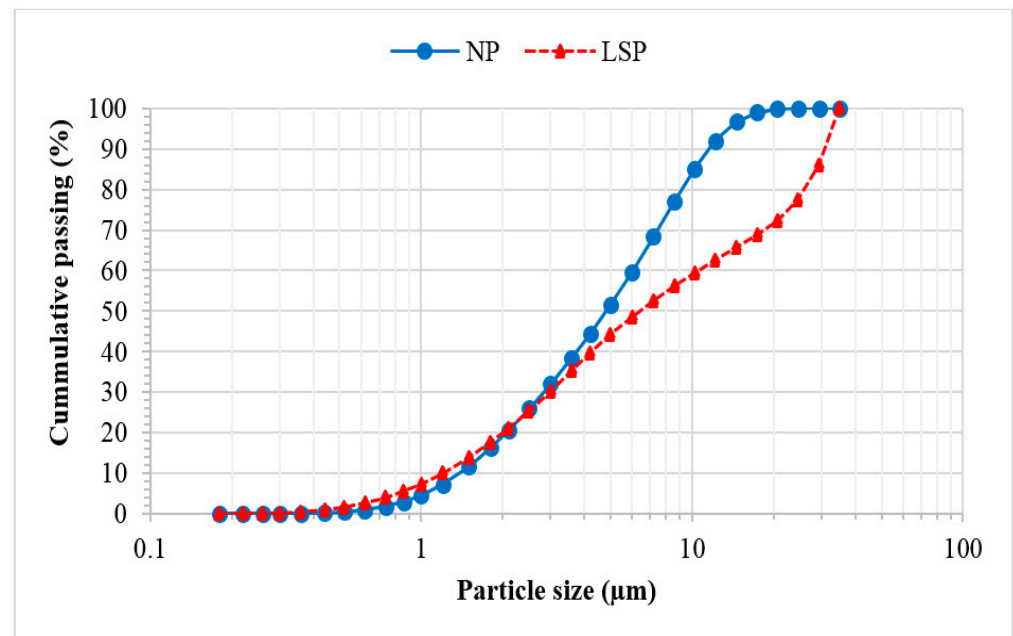

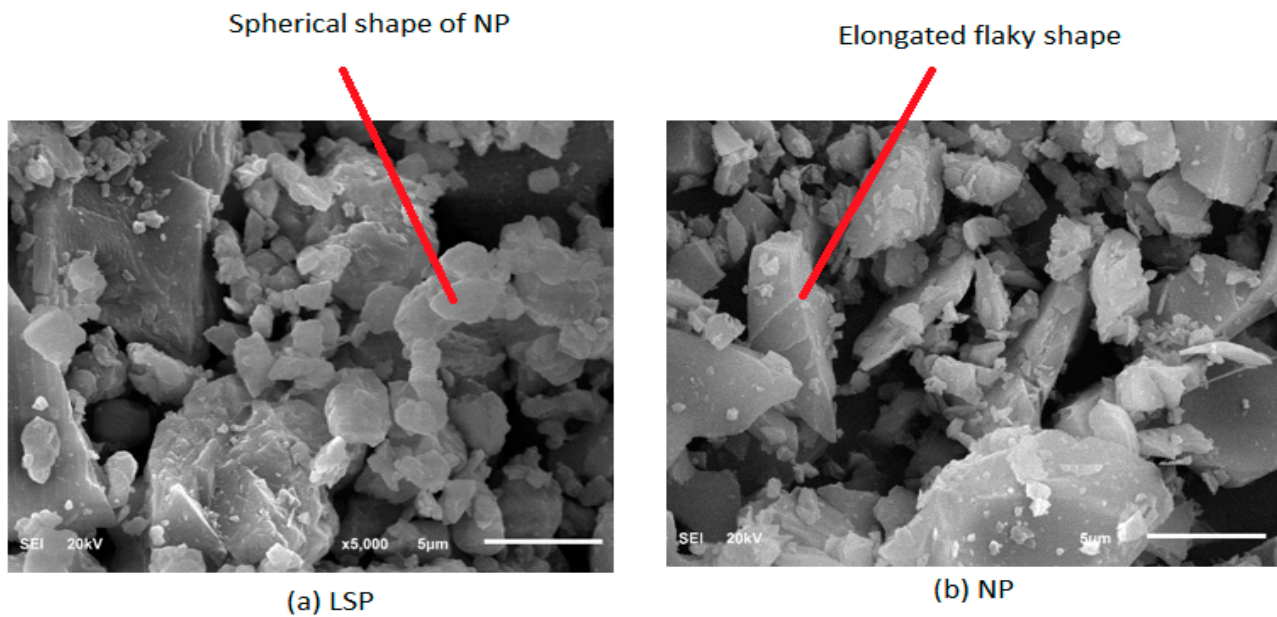**Figure 1.** NP and LSP particle size distribution.
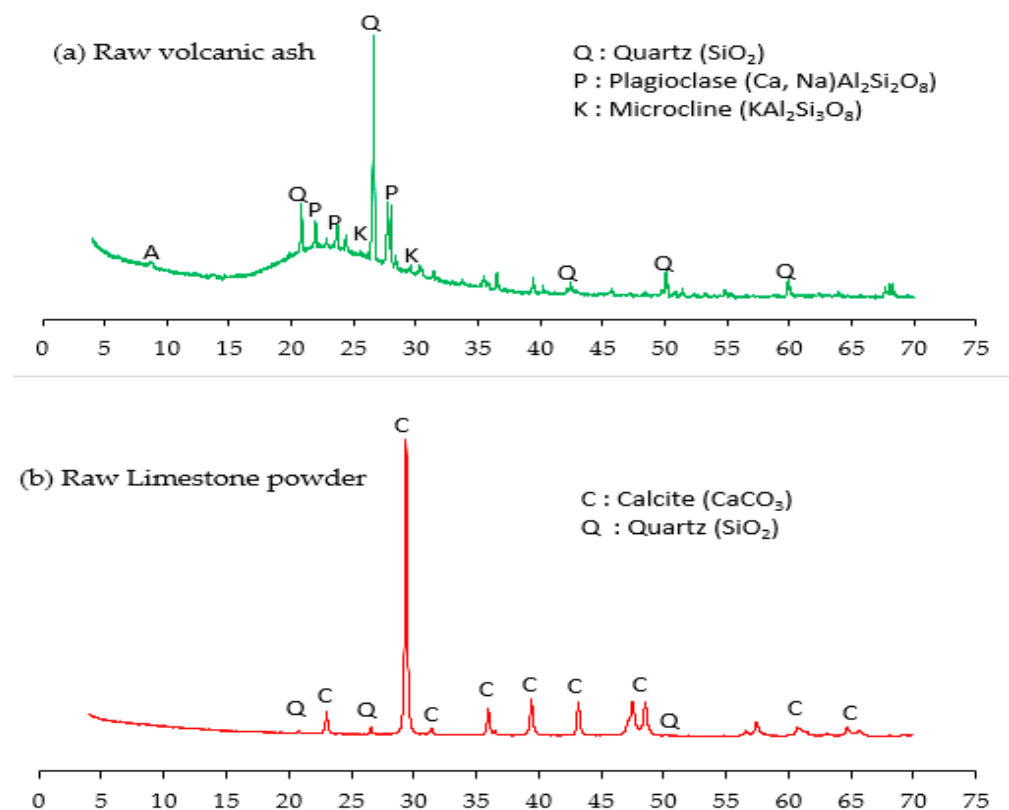
Figure 2. Micrograph images.

Figure 3. XRD: (**a**) NP and (**b**) LSP.

3.2. Effect of Binder Combination on Absorption

Figure 4 shows the absorption rate of the alkaline-activated mortar with different NP/LSP binder ratios ($AAN_{40}L_{60}$, $AAN_{50}L_{50}$, $AAN_{60}L_{40}$). The absorption rate increased as the immersion duration increased but decreased as the NP/LSP ratio increased such that the increment in NP/LSP from 0.67 to 1.0 and 1.5 led to 3.16% and 6.8% moisture contents, respectively. The sample with the high-volume NP ($AAN_{60}L_{40}$) had the highest absorption value; this can be attributed to the higher specific surface area of NP (3.1 cm^2/g) (Table 1)

and the angular flaky shape of LSP, as revealed in the SEM results shown in Figure 2. The preponderance of NP over LSP ($AAN_{60}L_{40}$) makes the mortar more porous, thereby increasing its absorption capacity.
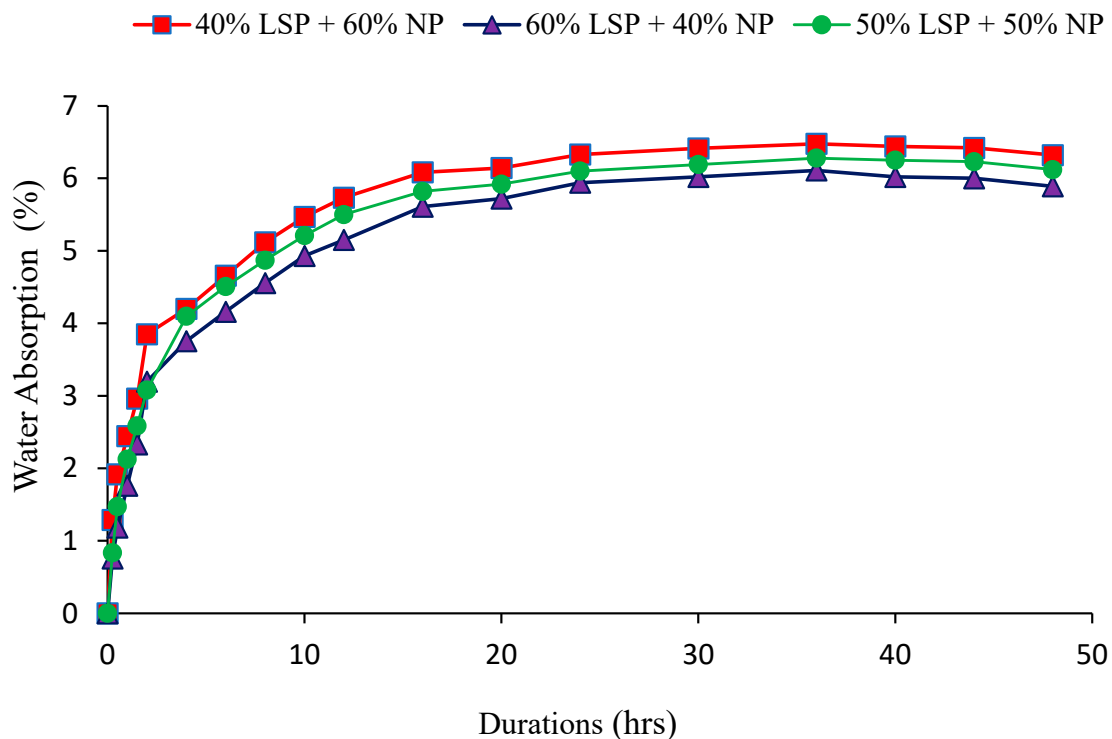
Figure 4. Effect of binder combination on absorption.

3.3. Visual Characterization in Acidic Exposure

The visual examination of the AANL mortar mixtures after one year of exposure to an acid solution (6% H_2SO_4) is depicted in Figure 5. It was observed that $AAN_{60}L_{40}$ exhibited little surface deterioration after 12 months in acid solution, unlike $AAN_{50}L_{50}$, whose surface became gritty after 12 months of exposure with minor surface distortion. When the NP content was further reduced to 40% ($AAN_{40}L_{60}$), the sample exhibited major surface deterioration and cracks with edge delamination. This implies that the sample with a high volume of NP showed better resistance to acid attack than the sample with a high volume of limestone powder.
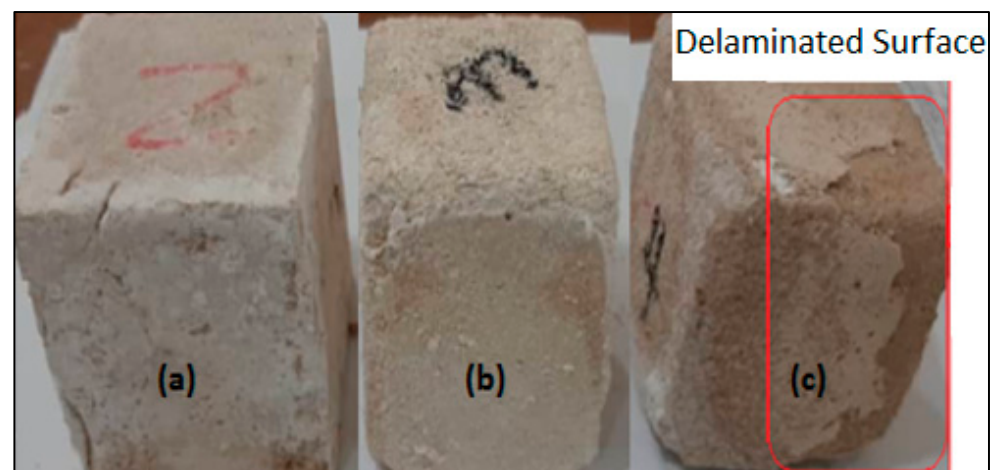

Figure 5. Visual examination of samples exposed to 6% H_2SO_4 attack: (**a**) $AAN_{60}L_{40}$, (**b**) $AAN_{50}L_{50}$, and (**c**) $AAN_{40}L_{60}$.

3.4. Effect of Binder Combination on Change in Weight of acid Exposed Specimen

Figure 6 shows the samples exposed to 6% H_2SO_4 for 3 months; all the specimens, i.e., $AAN_{40}L_{60}$, $AAN_{50}L_{50}$, and $AAN_{60}L_{40}$, experienced weight gain. However, after 6 months of exposure, the samples experienced weight reduction by 23%, 31.12%, and 12.7%, respectively. After 9 months of exposure, $AAN_{40}L_{60}$ and $AAN_{50}L_{50}$ experienced substantial losses in weight, while $AAN_{60}L_{40}$ exhibited marginal weight loss. $AAN_{40}L_{60}$ and $AAN_{50}L_{50}$ deteriorated further after 12 months, with weight loss of 10.59% and 7.62%, respectively, while $AAN_{60}L_{40}$ maintained its stability. This shows that high-volume natural pozzolan with high silica content enhanced the corrosion resistance against acid attack.
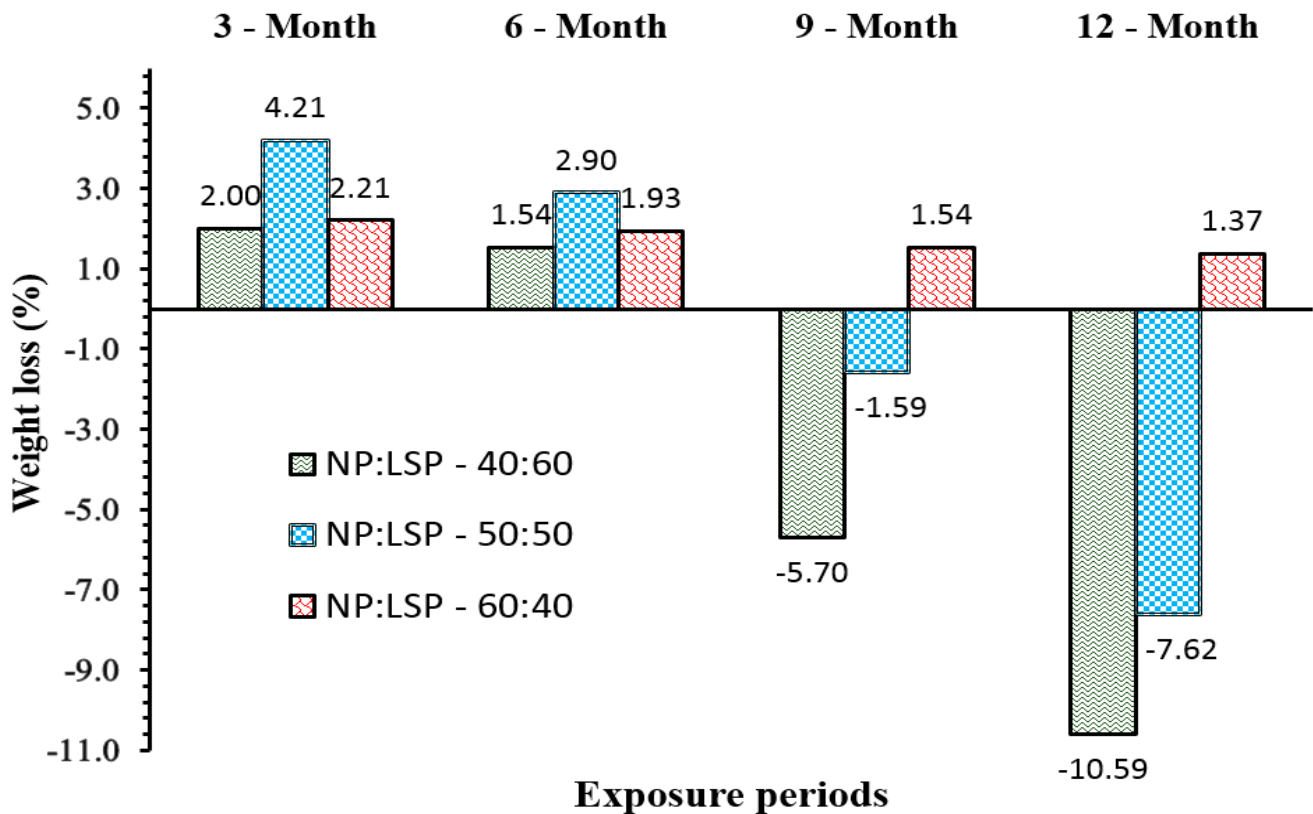
Figure 6. Change in weight of samples exposed to 6% H_2SO_4.

3.5. Residual Compressive Strength after Acid Attack

The residual compressive strengths of mortar mixtures exposed to 6% H_2SO_4 for 3, 6, 9, and 12 months are shown in Figure 7. Comparing the strength values of 28 days to various months of exposure, it was observed that for all samples exposed to acid attack (Figure 7), there was a sharp reduction in the compressive strength recorded throughout the exposure period, except for $AAN_{60}L_{40}$. The $AAN_{40}L_{60}$ sample experienced the highest residual strength loss of 75.56%, as shown in Figure 8, while $AAN_{60}L_{40}$ had the lowest loss of 16.80% after one year of exposure. At the balanced proportion of NP and LSP, the strength loss was 34%, 42%, 53%, and 69% for 3, 6, 9, and 12 months, respectively (Figure 8). There was no significant difference between the strength loss at 6 and 9 months in $AAN_{60}L_{40}$. Generally, the sample synthesized with a high volume of limestone (LSP) powder showed less resistance to acid attack, whereas $AAN_{60}L_{40}$ with a high volume of natural pozzolan (NP) exhibited the highest resistance to acid attack.
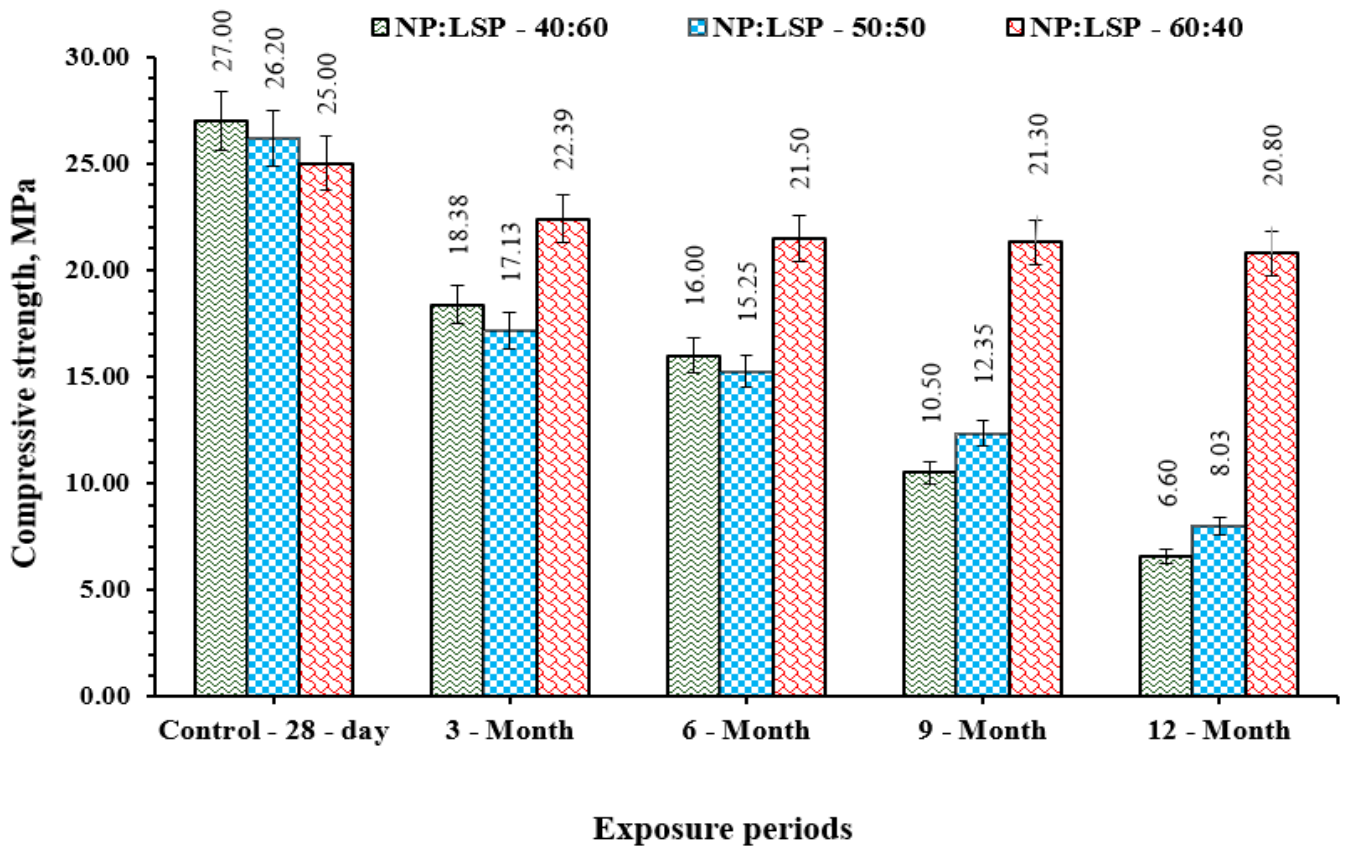
Figure 7. Compressive strength of samples exposed to 6% H_2SO_4.

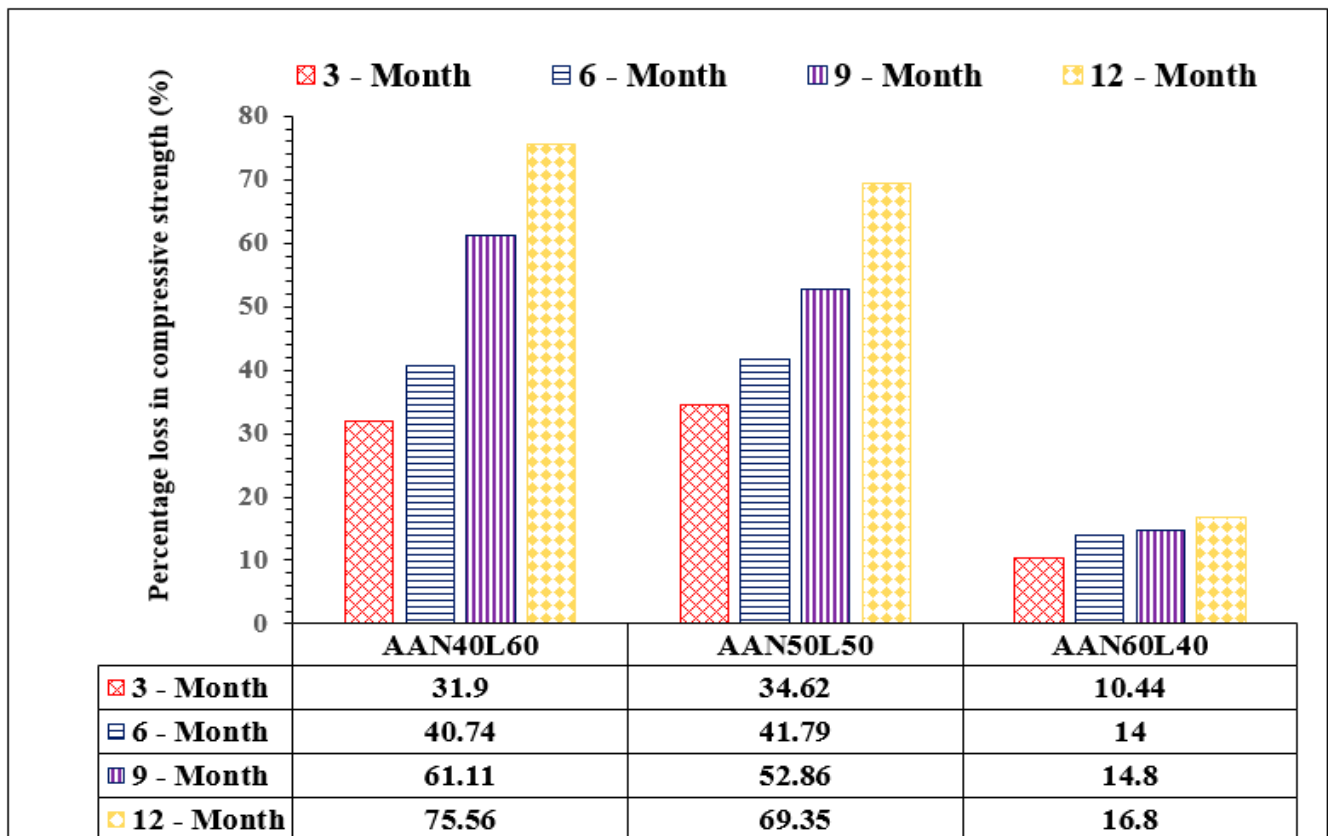|	AAN40L60	AAN50L50	AAN60L40
3 – Month	31.9	34.62	10.44
6 – Month	40.74	41.79	14
9 – Month	61.11	52.86	14.8
12 – Month	75.56	69.35	16.8

Figure 8. Percentage loss in compressive strength with 1 year of exposure to acid attack.

3.6. Mineralogy, Morphology, and Bond Characteristics of Mortar after Exposure to Acid Environment

3.6.1. XRD Characterization of AANL Binder

The XRD spectra of the exposed and unexposed binder are depicted in Figure 9. $AAN_{60}L_{40}$, $AAN_{50}L_{50}$, and $AAN_{40}L_{60}$ have almost similar microstructural characteristics before exposure to a severe acidic environment, as reflected in the compressive strength results (Figure 7); thus, $AAN_{40}L_{60}$ is used as the control for the unexposed samples. The alkaline activators can dissolve complex aluminosilicate present in the base materials to release monomers that come together to form the product through condensation, as shown in Equations (4)–(6). The alkaline-activated products formed are gehlenite ($Ca0.Al_2O_3.SiO_2$), anorthite ($CaAl_2Si_2O_8$), and albite ($NaAlSi_3O_8$) (Figure 9a).

$$CaCO_3 \rightarrow CaO + CO_2 \tag{4}$$

$$Na_2SiO_{3(aq)} \rightarrow Na_2O + SiO_2 + H_2O \tag{5}$$

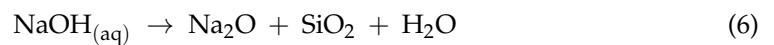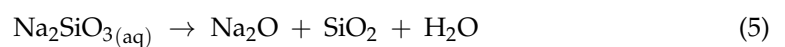$$NaOH_{(aq)} \rightarrow Na_2O + SiO_2 + H_2O \tag{6}$$
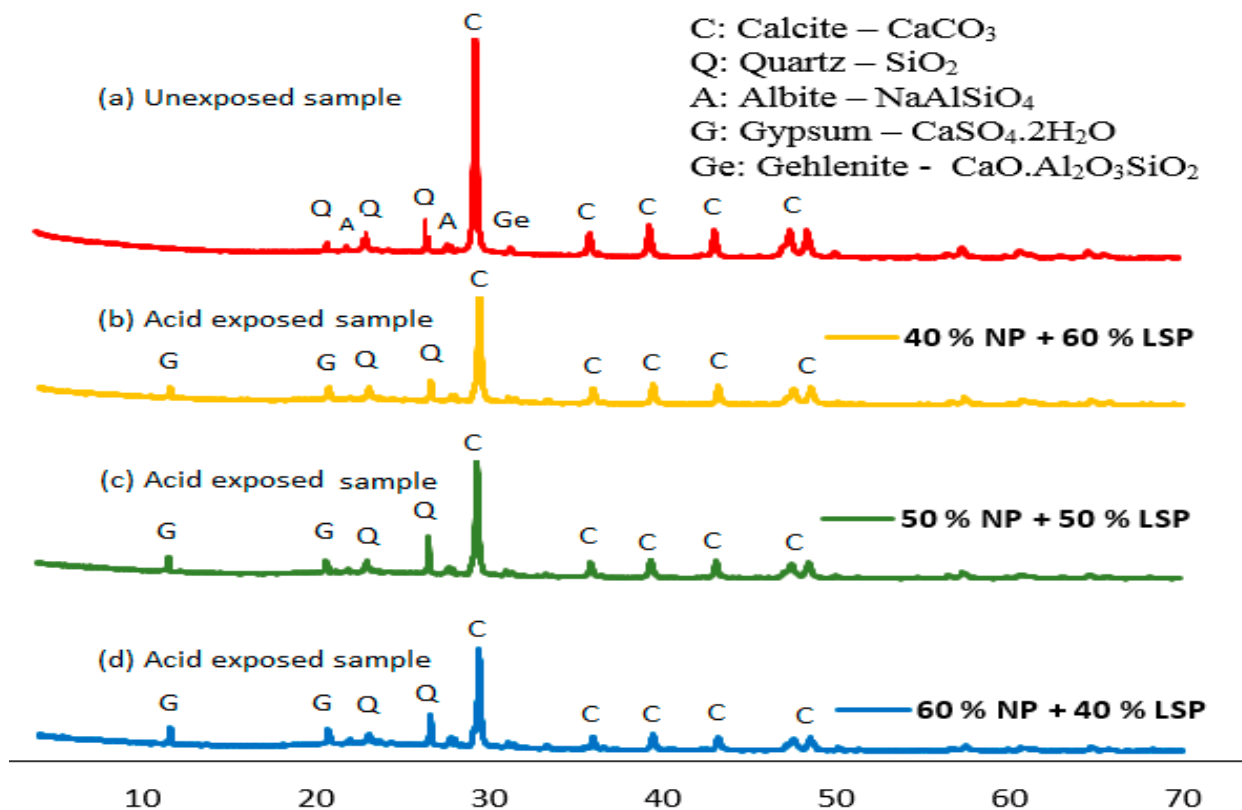
Figure 9. X-ray diffractograms of the exposed and unexposed samples.

These products enhanced the strength development, but exposure to sulfuric acid destroyed phases such as gehlenite and albite in the LSP-dominated binder, as shown in Figure 9. The destruction of gehlenite and albite could be due to ion exchange between hydroxonium ion of an acid and calcium in LSP to form gypsum, as shown in Equation (7).

$$CaCO_3 + H_2SO_4 + H_2O \rightarrow CaSO_4.2H_2O + CO_2 \tag{7}$$
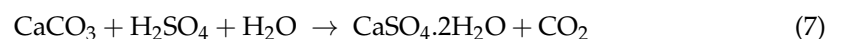
The formation of gypsum on all the tested binders after acidic exposure is evidenced in Figure 9b,c. The gypsum formed caused leaching of the alkali-activated product, subsequently leading to mass and strength reduction in the mortar; however, this effect is not prominent in the binder developed with a high content of NP ($AAN_{60}L_{40}$).

3.6.2. FTIR Analysis of Samples after Acid Attack

Figure 10 shows the FTIR image of the mortar before and after exposure to sulfuric acid attack. The major functional groups affected were the hydroxyl group, binding water present within the pores, and Si-O-Si reorganization. The wavenumbers at 3500 cm^{-1} and 2375 cm^{-1} showing the presence of hydroxyl group (O-H) stretching and water molecule (H-O-H) bending at the wavenumbers of 1645 cm^{-1} were observed in the unexposed samples (Figure 10a). A stretching vibration of C-O-O (CO_3^{2-}) was observed at a wavenumber of 1418 cm^{-1} in the unexposed sample. However, upon exposure to the acidic environment, the broad peak of the hydroxyl group was decomposed due to acid attack, as revealed in Figure 10b–d. Furthermore, the H-O-H bending at wavenumber 2335 cm^{-1} in the unexposed sample changed to a deeper peak due to the precipitation of more water molecules entrapped in the binder matrix due to $H_2SO_{4(aq)}$. The carbonyl group around 1427 cm^{-1} in the unexposed sample was observed to be depleted after acid attack.
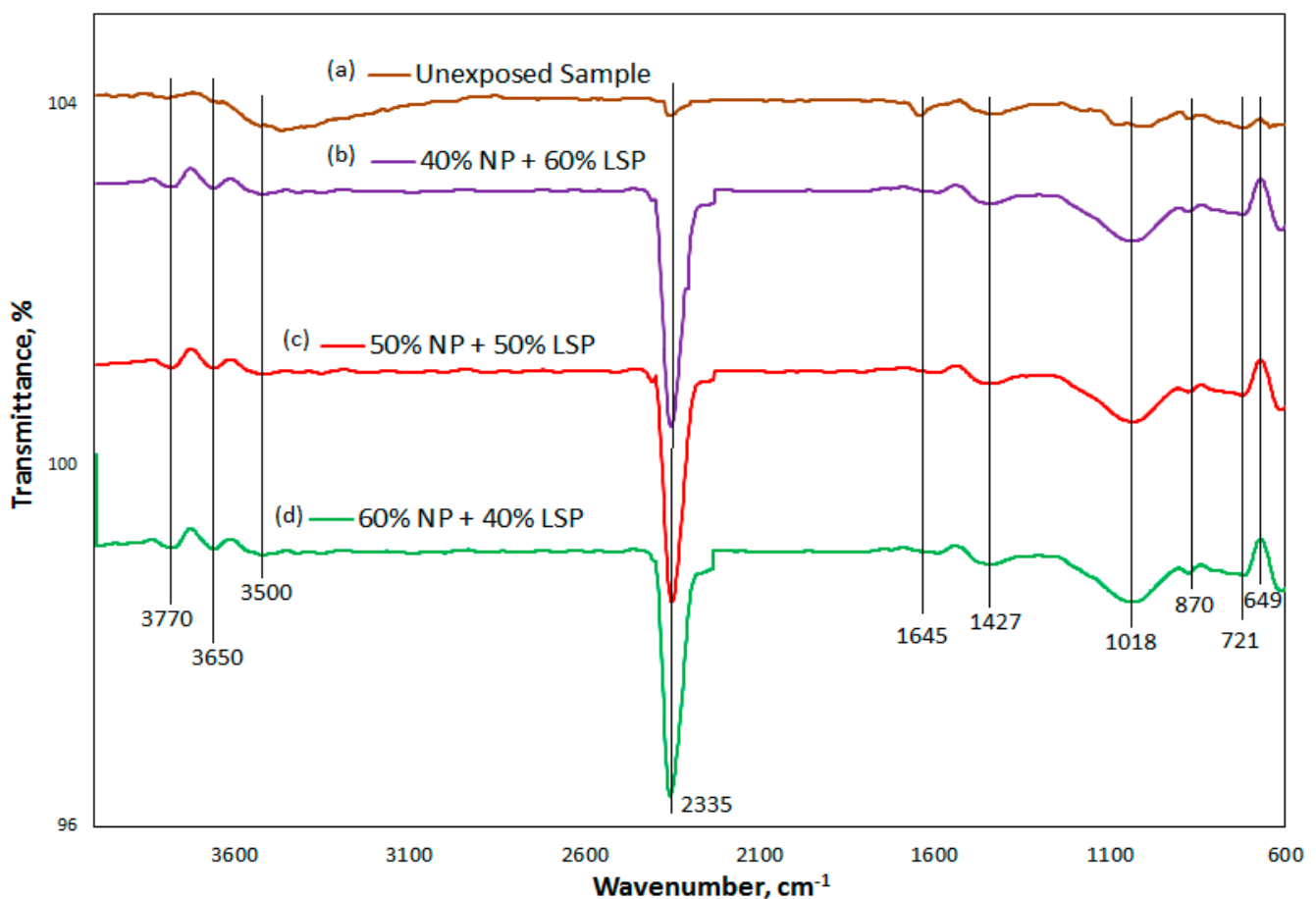

Figure 10. FTIR spectra of specimen unexposed and exposed to 6% H_2SO_4.

Furthermore, the intensity band of Si-O-T from the aluminosilicate framework at 1018 cm^{-1} due to asymmetric vibration, which corresponds to binder gel, becomes broadened after acid attack. This implies that the depolymerization of C-A-S-H and N-A-S-H products occurred due to the elimination of Al and Si atoms from the binder. A weak absorption band of dihydrate gypsum (S-O) at a wavenumber of 649 cm^{-1} was also found in the exposed samples, whereas it was absent in the unexposed samples. For the unexposed sample, in-plane bending vibration of C-O was found in a weak absorption peak of 721 cm^{-1}, and this was shifted to a lower band of 711 cm^{-1}. The high strength loss recorded in AAN$_{60}$L$_{40}$ and AAN$_{50}$L$_{50}$ exposed samples is caused by the formation of gypsum after decalcification of the binder matrix, while the marginal strength loss in

$AAN_{60}L_{40}$ is due to the presence of high silica content that hindered high degradation of the aluminosilicate framework.

3.6.3. SEM and EDX Analysis of Samples after Acid Attack

Figures 11–14 depict the SEM and EDS findings for the AANL binder under acidic and non-acidic conditions. The control sample's SEM image showed a uniform and denser microstructure as a result of more alkaline-activated product production (Figure 11). From the EDS (unexposed sample) results, the Si/Na values of 0.96–1.4, Si/Ca = 0.84–2.33 and Si/Al = 4.84–7.11 were noted in spectra 5 and 6 (Figure 11). This indicates the formation of aluminosilicate products such as C-A-S-H and N-A-S-H, thereby enhancing strength development.

However, after exposure to 6% H_2SO_4 for 1 year, spectrum 4 of $AAN_{60}L_{40}$ (Figure 14) exposed to acid attack showed the presence of gypsum, C-A-S-H, and N-A-S-H products with a dense microstructure. The exposed sample EDS results show that the Si/Al ratio decreases with an increased in the percentage of NP. The highest value of Si/Na = 8.7, was observed on spectrum 17 for $AAN_{40}L_{60}$ (Figure 13); Si/Na = 7.2 for $AAN_{50}L_{50}$, as shown in spectrum 10 (Figure 14) and Si/Na = 6.6 for $AAN_{60}L_{40}$, as depicted in spectrum 3 (Figure 14). Furthermore, there was a higher Ca/Si ratio of 10.5 in $AAN_{60}L_{40}$, as revealed in spectrum 3, than in $AAN_{50}L_5$ (spectrum 10), with Ca/Si = 0.5. For $AAN_{40}L_{60}$, as shown in spectrum 18, Ca/Si = 2.1. $AAN_{60}L_{40}$ with the highest value of Ca/Si and the lowest value of Si/Al had the highest resistance to H_2SO_4, with residual compressive strength of 20.8 MPa after 1 year of exposure to acid attack. $AAN_{40}L_{60}$ and $AAN_{50}L_{50}$ have a porous microstructure, as shown in the magnified micrographs (Figures 13b and 14b), which accounted for the loss in strength recorded.
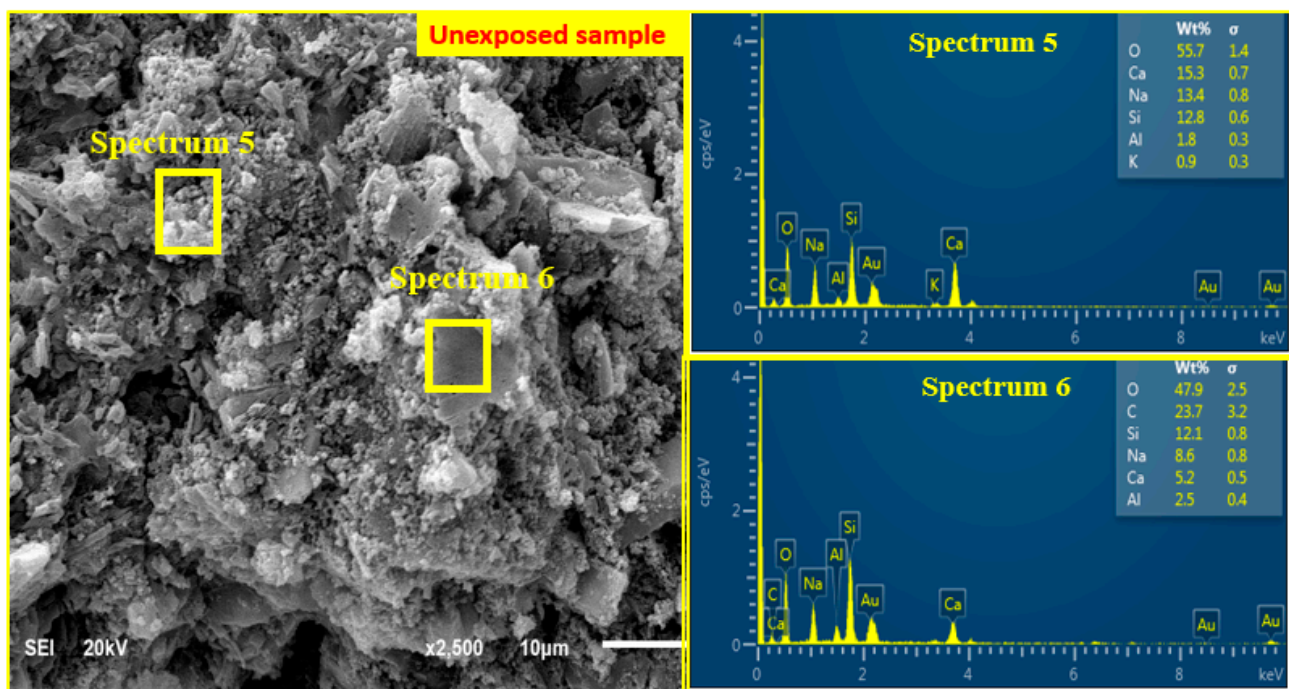

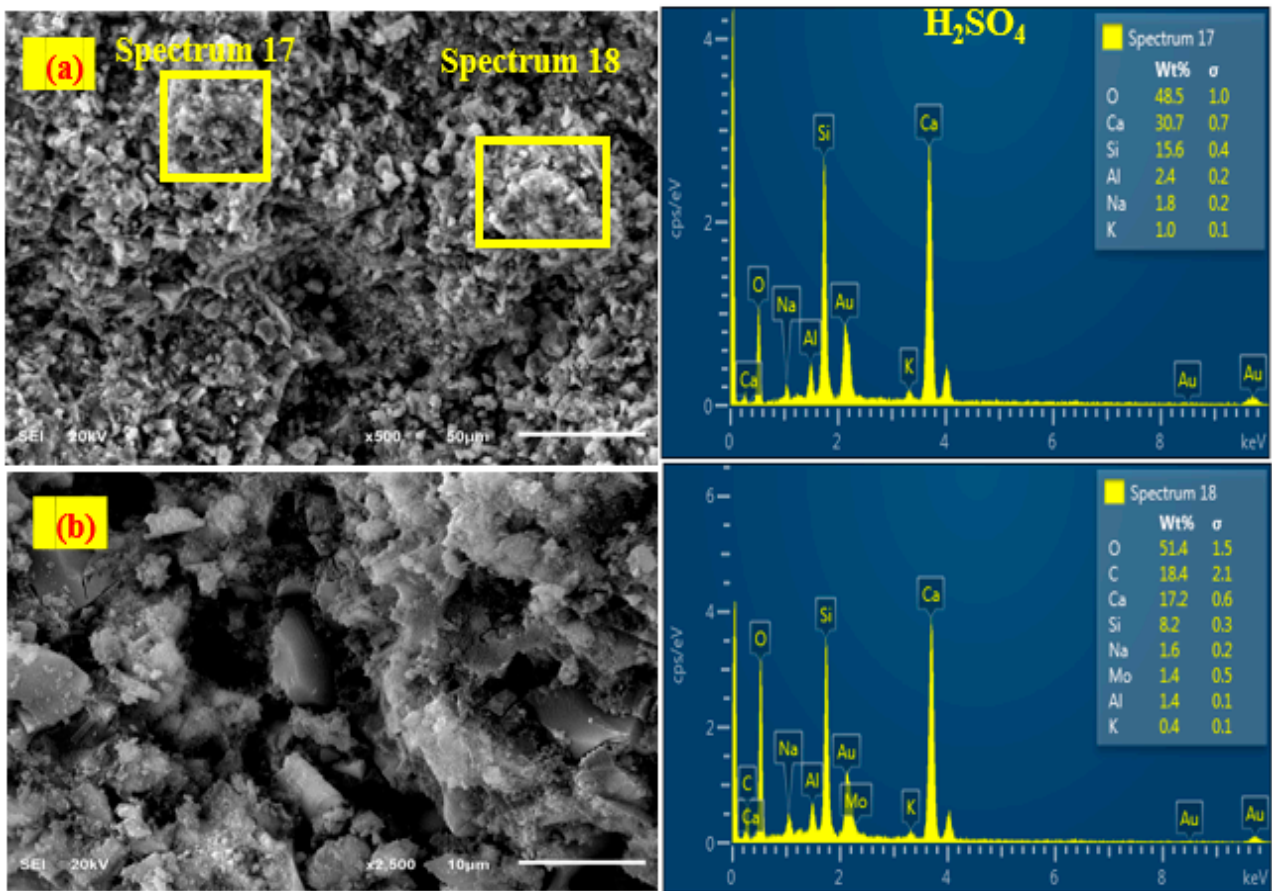**Figure 11.** SEM and EDS of unexposed control sample.

Figure 12. SEM and EDS of AAN$_{40}$L$_{60}$ exposed to 6% H$_2$SO$_4$: (**a**) low magnification; (**b**) high magnification.
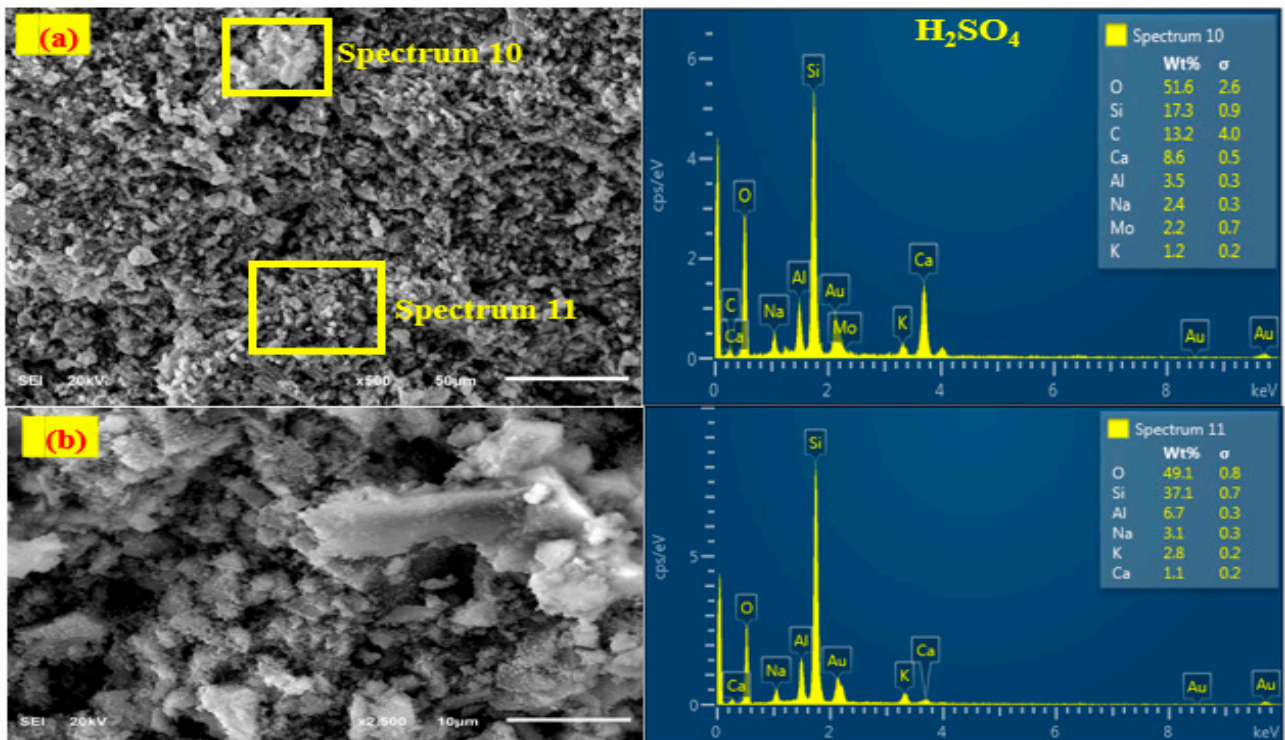
Figure 13. SEM and EDS of AAN$_{50}$L$_{50}$ exposed to 6% H$_2$SO$_4$: (**a**) low magnification; (**b**) high magnification.
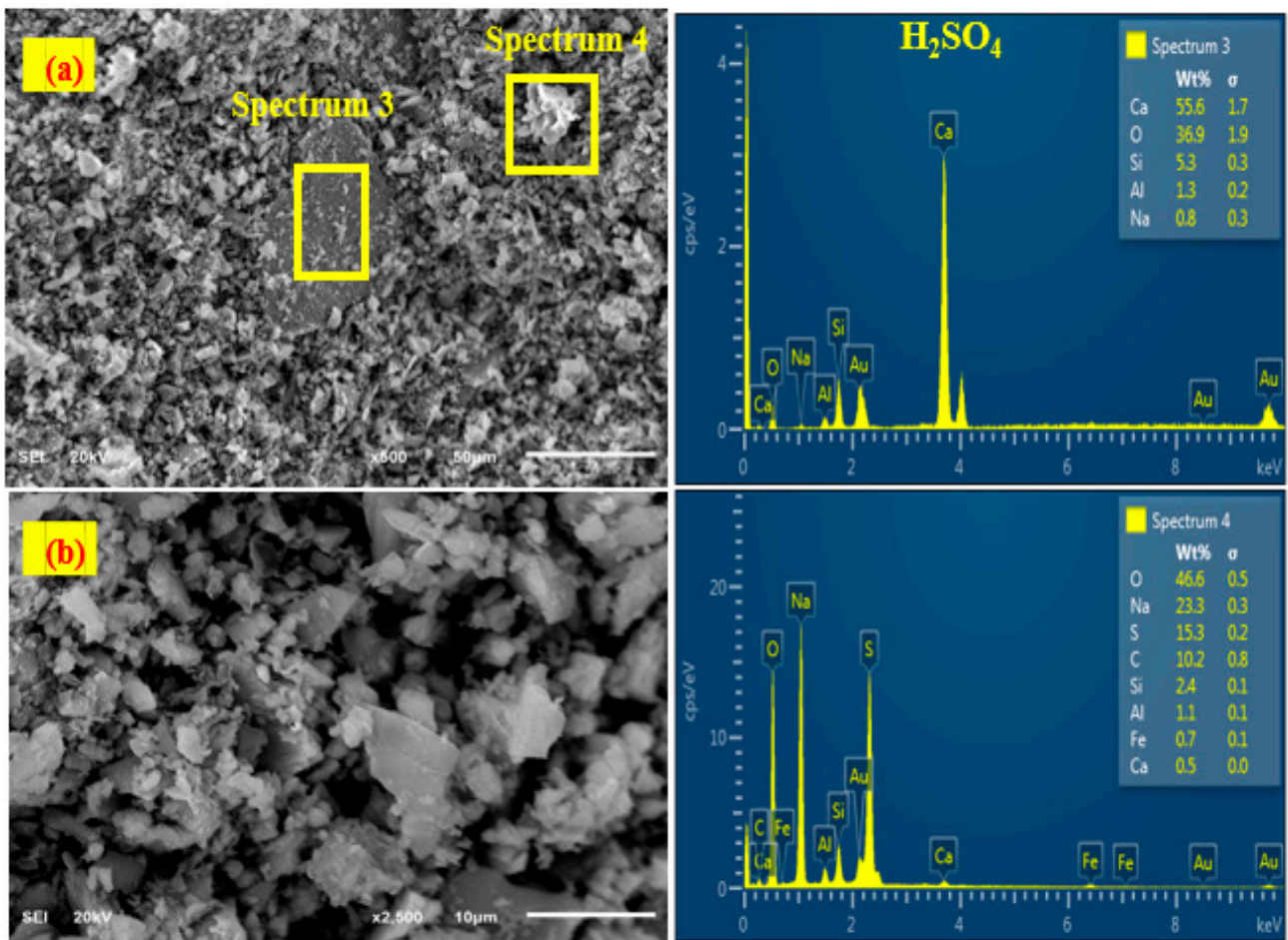
Figure 14. SEM and EDS of $AAN_{60}L_{40}$ exposed to 6% H_2SO_4: (**a**) low magnification; (**b**) high magnification.

4. Conclusions

The impacts of high-volume natural pozzolan on the sulfuric acidic resistance of alkali-activated mortar after 1 year of exposure to sulfuric acid are summarized as follows.

1. The mortar exhibited more expansion in the presence of a low volume of NP.
2. The maximum strengths of 20.8 MPa and 6.68 MPa were noted in mortar developed using a high volume of NP ($AAN_{60}L_{40}$) and a low volume of NP ($AAN_{40}L_{60}$), respectively.
3. The ultimate residual strengths were 16.8% and 1.4% for $AAN_{60}L_{40}$ and $AAN_{40}L_{60}$, respectively.
4. The mass gains were 75.6% and −10.64% for $AAN_{60}L_{40}$ and $AAN_{40}L_{60}$, respectively.
5. Samples synthesized using $AAN_{60}L_{40}$ (60% NP:40% LSP) exhibited no surface deterioration, while samples synthesized using $AAN_{40}L_{60}$ (40% NP:60% LSP) exhibited major surface cracks with minor multiple-edge delamination.
6. The high sulfuric acid resistance of $AAN_{60}L_{40}$ mortar is attributed to the presence of high values of Si/Al = 7 and Ca/Si = 10 present in C-A-S-H and N-A-S-H products, which resulted in the pore-filling effects within the microstructure.
7. The low strength recorded in $AAN_{40}L_{60}$ was due to the formation of gypsum in the binder product, whereas samples synthesized with a high volume of natural pozzolan ($AAN_{60}L_{40}$) showed more stability against acid attack.
8. $AAN_{60}L_{40}$ exhibited the highest resistance to sulfuric acid attack.

References

1. Godinho, J.P.; de Medeiros, M.H.F. Biogenic sulfur attack in a reinforced concrete sewage treatment plant. Re-visited mechanism and rehabilitation proposal. *Eng. Fail. Anal.* **2021**, *124*, 105354. [CrossRef]
2. Madhuri, P.; Rao, B.K.; Chaitanya, A. Improved performance of concrete incorporated with natural zeolite powder as supplementary cementitious material. *Mater. Today Proc.* **2021**, *47*, 5369–5378. [CrossRef]
3. Mustapha, F.A.; Sulaiman, A.; Mohamed, R.; Umara, S. The effect of fly ash and silica fume on self-compacting high-performance concrete. *Mater. Today Proc.* **2020**, *39*, 965–969. [CrossRef]
4. Du, H.; Pang, S.D. Long-Term Influence of Nanosilica on the Microstructures, Strength, and Durability of High-Volume Fly Ash Mortar. *J. Mater. Civ. Eng.* **2021**, *33*, 04021185. [CrossRef]
5. Liu, S.; Zhu, M.; Ding, X.; Ren, Z.; Zhao, S.; Zhao, M.; Dang, J. High-Durability Concrete with Supplementary Cementitious Admixtures Used in Corrosive Environments. *Crystals* **2021**, *11*, 196. [CrossRef]
6. Kumar, M.; Sinha, A.K.; Kujur, J. Mechanical and durability studies on high-volume fly-ash concrete. *Struct. Concr.* **2020**, *22*, E1036–E1049. [CrossRef]
7. Huseien, G.F.; Joudah, Z.H.; Khalid, N.H.A.; Sam, A.R.M.; Tahir, M.M.; Lim, N.H.A.S.; Alyousef, R.; Mirza, J. Durability performance of modified concrete incorporating fly ash and effective microorganism. *Constr. Build. Mater.* **2021**, *267*, 120947. [CrossRef]
8. AlBiajawi, M.I.; Embong, R.; Muthusamy, K. An overview of the utilization and method for improving pozzolanic performance of agricultural and industrial wastes in concrete. *Mater. Today Proc.* **2021**, *48*, 778–783. [CrossRef]
9. Raheem, A.; Abdulwahab, R.; Kareem, M. Incorporation of metakaolin and nanosilica in blended cement mortar and concrete- A review. *J. Clean. Prod.* **2021**, *290*, 125852. [CrossRef]
10. Elavarasan, S.; Priya, A.; Ajai, N.; Akash, S.; Annie, T.; Bhuvana, G. Experimental study on partial replacement of cement by metakaolin and GGBS. *Mater. Today Proc.* **2020**, *37*, 3527–3530. [CrossRef]
11. Tambe, Y.; Nemade, P. Performance of Conventional Concrete Integrated with RHA and GGBS As a Cementitious Material. *Techno Soc.* **2020**, *2021*, 341–353. [CrossRef]
12. Sata, V.; Sathonsaowaphak, A.; Chindaprasirt, P. Resistance of lignite bottom ash geopolymer mortar to sulfate and sulfuric acid attack. *Cem. Concr. Compos.* **2012**, *34*, 700–708. [CrossRef]
13. Bakharev, T. Resistance of geopolymer materials to acid attack. *Cem. Concr. Res.* **2005**, *35*, 658–670. [CrossRef]
14. Tho-In, T.; Sata, V.; Chindaprasirt, P.; Jaturapitakkul, C. Pervious high-calcium fly ash geopolymer concrete. *Constr. Build. Mater.* **2012**, *30*, 366–371. [CrossRef]
15. Chen, K.; Wu, D.; Yi, M.; Cai, Q.; Zhang, Z. Mechanical and durability properties of metakaolin blended with slag geopolymer mortars used for pavement repair. *Constr. Build. Mater.* **2021**, *281*, 122566. [CrossRef]
16. Ren, J.; Zhang, L.; Nicolas, R.S. Degradation of Alkali-Activated Slag and Fly Ash Mortars under Different Aggressive Acid Conditions. *J. Mater. Civ. Eng.* **2021**, *33*, 04021140. [CrossRef]
17. Wang, A.; Zheng, Y.; Zhang, Z.; Liu, K.; Li, Y.; Shi, L.; Sun, D. The Durability of Alkali-Activated Materials in Comparison with Ordinary Portland Cements and Concretes: A Review. *Engineering* **2020**, *6*, 695–706. [CrossRef]
18. Salami, B.A.; Johari, M.A.M.; Ahmad, Z.A.; Maslehuddin, M. POFA-Engineered Alkali-activated Cementitious Composite Performance in Acid Environment. *J. Adv. Concr. Technol.* **2017**, *15*, 684–699. [CrossRef]
19. Idir, R.; Cyr, M.; Pavoine, A. Investigations on the durability of alkali-activated recycled glass. *Constr. Build. Mater.* **2019**, *236*, 117477. [CrossRef]
20. Joudah, Z.H.; Huseien, G.F.; Samadi, M.; Lim, N.H.A.S. Sustainability evaluation of alkali-activated mortars incorporating industrial wastes. *Mater. Today Proc.* **2021**, *46*, 1971–1977. [CrossRef]

21. Huseien, G.F.; Sam, A.R.M.; Shah, K.W.; Mirza, J.; Tahir, M.M. Evaluation of alkali-activated mortars containing high volume waste ceramic powder and fly ash replacing GBFS. *Constr. Build. Mater.* **2019**, *210*, 78–92. [CrossRef]

22. Jeon, I.K.; Kim, H.G.; Jakhrani, S.H.; Ryou, J.-S. Evaluation of the microstructure, mechanical, and durability properties of alkali-activated slag-based mortar with light-burnt dolomite powder. *J. Mater. Res. Technol.* **2021**, *13*, 2220–2228. [CrossRef]

23. Sasui, S.; Kim, G.; Nam, J.; van Riessen, A.; Hadzima-Nyarko, M. Effects of waste glass as a sand replacement on the strength and durability of fly ash/GGBS based alkali activated mortar. *Ceram. Int.* **2021**, *47*, 21175–21196. [CrossRef]

24. Yang, Y.; Zeng, H.; Chang, J.; Shi, J.; Liu, B. Waste glass powder and its effect on the fresh and mechanical properties of concrete: A state of the art review. *Adv. Concr. Constr.* **2020**, *10*, 417–429. [CrossRef]

25. Tome, S.; Nana, A.; Kaze, C.R.; Djobo, J.N.Y.; Alomayri, T.; Kamseu, E.; Etoh, M.-A.; Etame, J.; Kumar, S. Resistance of Alkali-Activated Blended Volcanic Ash-MSWI-FA Mortar in Sulphuric Acid and Artificial Seawater. *Silicon* **2021**, *14*, 2687–2694. [CrossRef]

26. Kaze, C.R.; Tome, S.; Lecomte-Nana, G.L.; Adesina, A.; Essaedi, H.; Das, S.K.; Alomayri, T.; Kamseu, E.; Melo, U.C. Development of alkali-activated composites from calcined iron-rich laterite soil. *Materialia* **2021**, *15*, 101032. [CrossRef]

27. Nasir, M.; Johari, M.A.M.; Maslehuddin, M.; Yusuf, M.O. Magnesium sulfate resistance of alkali/slag activated silico-manganese fume-based composites. *Constr. Build. Mater.* **2020**, *265*, 120851. [CrossRef]

28. Bailey, R.A.; Clark, H.M.; Ferris, J.P.; Krause, S.; Strong, R.L. *Chemistry and Environment*; Elsevier: Amsterdam, The Netherlands, 2002; pp. 443–482. Available online: https://www.elsevier.com/books/chemistry-of-the-environment/9780120734610 (accessed on 31 October 2022).

29. Adewumi, A.A.; Ariffin, M.A.M.; Yusuf, M.O.; Maslehuddin, M.; Ismail, M. Effect of sodium hydroxide concentration on strength and microstructure of alkali-activated natural pozzolan and limestone powder mortar. *Constr. Build. Mater.* **2020**, *271*, 121530. [CrossRef]

30. Silva, G.; Castañeda, D.; Kim, S.; Castañeda, A.; Bertolotti, B.; Ortega-San-Martin, L.; Nakamatsu, J.; Aguilar, R. Analysis of the production conditions of geopolymer matrices from natural pozzolana and fired clay brick wastes. *Constr. Build. Mater.* **2019**, *215*, 633–643. [CrossRef]

31. Firdous, R.; Stephan, D. Effect of silica modulus on the geopolymerization activity of natural pozzolans. *Constr. Build. Mater.* **2019**, *219*, 31–43. [CrossRef]

32. Mageed, A.A.; AbdelHaffez, S. Utilization of Limestone Dust in Brick Making. *J. Eng. Sci.* **2012**, *40*, 913–922.

33. Ghafoori, N.; Najimi, M.; Radke, B. Natural Pozzolan-based geopolymers for sustainable construction. *Environ. Earth Sci.* **2016**, *75*, 1110. [CrossRef]

34. Ibrahim, M.; Johari, M.A.M.; Maslehuddin, M.; Rahman, M.K.; Salami, B.A.; Mohamed, H.D. Influence of composition and concentration of alkaline activator on the properties of natural-pozzolan based green concrete. *Constr. Build. Mater.* **2019**, *201*, 186–195. [CrossRef]

35. Ibrahim, M.; Salami, B.A.; Algaifi, H.A.; Rahman, M.K.; Nasir, M.; Ewebajo, A.O. Assessment of acid resistance of natural pozzolan-based alkali-activated concrete: Experimental and optimization modelling. *Constr. Build. Mater.* **2021**, *304*, 124657. [CrossRef]

36. Ibrahim, M.; Johari, M.A.M.; Rahman, M.K.; Maslehuddin, M. Effect of alkaline activators and binder content on the properties of natural pozzolan-based alkali activated concrete. *Constr. Build. Mater.* **2017**, *147*, 648–660. [CrossRef]

37. Ibrahim, M.; Rahman, M.K.; Johari, M.A.M.; Maslehuddin, M. Effect of Incorporating Nano-silica on the Strength of Natural Pozzolan-Based Alkali-Activated Concrete. In *International Congress on Polymers in Concrete (ICPIC 2018)*; Springer International Publishing: Berlin/Heidelberg, Germany, 2018; pp. 703–709. [CrossRef]

38. Ghasemi, M.; Rasekh, H.; Berenjian, J.; AzariJafari, H. Dealing with workability loss challenge in SCC mixtures incorporating natural pozzolans: A study of natural zeolite and pumice. *Constr. Build. Mater.* **2019**, *222*, 424–436. [CrossRef]

39. Aragón, P.; Robayo-Salazar, R.A.; de Gutiérrez, R.M. Alkali-Activated Concrete Based on Natural Volcanic Pozzolan: Chemical Resistance to Sulfate Attack. *J. Mater. Civ. Eng.* **2020**, *32*, 04020106. [CrossRef]

40. Djobo, J.N.Y.; Elimbi, A.; Tchakouté, H.K.; Kumar, S. Mechanical properties and durability of volcanic ash based geopolymer mortars. *Constr. Build. Mater.* **2016**, *124*, 606–614. [CrossRef]

41. Bondar, D.; Lynsdale, C.J.; Milestone, N.B.; Hassani, N. Sulfate Resistance of Alkali Activated Pozzolans. *Int. J. Concr. Struct. Mater.* **2014**, *9*, 145–158. [CrossRef]

42. Oxygen and Chloride Permeability of Alkali-Activated Natural Pozzolan Concrete. *ACI Mater. J.* **2012**, *109*, 53–62. [CrossRef]

43. Aguirre-Guerrero, A.M.; Robayo-Salazar, R.A.; de Gutiérrez, R.M. Corrosion resistance of alkali-activated binary reinforced concrete based on natural volcanic pozzolan exposed to chlorides. *J. Build. Eng.* **2020**, *33*, 101593. [CrossRef]

44. Ibrahim, M.; Rahman, M.K.; Johari, M.A.M.; Nasir, M.; Oladapo, E.A. Chloride diffusion and chloride-induced corrosion of steel embedded in natural pozzolan-based alkali activated concrete. *Constr. Build. Mater.* **2020**, *262*, 120669. [CrossRef]

45. Ozata, S.; Akturk, B.; Yuzer, N. Utilization of waste Cappadocia earth as a natural pozzolan in alkali activation: A parametric study. *Constr. Build. Mater.* **2022**, *329*, 127192. [CrossRef]